*pISSN 2508-1357, eISSN 2508-139X*
*J Biomed Transl Res 2020;21(2):079-090*
*https://doi.org/10.12729/jbtr.2020.21.2.079*
*Received 3 Jun. 2020, Accepted 9 Jun. 2020*

**Research Article**

# Radioisotope-ADME studies of Trastuzumab-monomethyl auristatin F in tumor bearing mice and healthy marmosets

Hye Won Lee[1], Yun Ha Jeong[2], Jin Ah Hwang[2], Jae Jun Lee[3], A-Ram Yu[3], Jung Ae Kang[3], Muhammad Asim Raza[4,5], Sang Hyun Park[4,5], Yun-Hee Park[6], Dong Hwan Kim[2*]

[1]*Department of Toxicology Evaluation, Graduate School of Konyang University, Daejeon 35365, Korea*
[2]*Department of Medicinal Biosciences, Konyang University, Nonsan 32992, Korea*
[3]*Laboratory Animal Center, Osong Medical Innovation Foundation, Cheongju 28160, Korea*
[4]*Advanced Radiation Technology Institute, Korea Atomic Energy Research Institute, Jeongeup 56212, Korea*
[5]*Radiation Science and Technology, University of Science and Technology, Daejeon 34113, Korea*
[6]*ADC Platform & R2D Team, LegoChem Biosciences, Inc., Daejeon 34302, Korea*

**Radioisotope ADME (RI-ADME) studies are enabling visualization of the biodistribution in molecular imaging. We applied RI-ADME to investigate the tumor targeting capacity and biodistribution of trastuzumab-monomethyl auristatin F (LCB14-0110) in JIMT-1 xenograft mice and healthy marmoset. The LCB14-0110 was labelled with $^{125}$I. $^{125}$I-LCB14-0110 was intravenously administered to the animals. The gamma-count and single-photon emission computed tomography/computed tomography (SPECT/CT) was conducted for biodistributioon and bioimaging of the biopharmaceutics. Tumor uptake in xenograft mice was highest at three-day after $^{125}$I-LCB14-0110 administration in both the biodistribution and SPECT/CT bioimaging. Alternatively, blood and organ tissues showed gradual decrease in radioactivity over time. In marmosets, radioactivity in all organ tissues rapidly reduced and no specific targeting of organs was observed in the biodistribution study and SPECT/CT imaging. Hence, $^{125}$I-LCB14-0110 demonstrated effective tumor targeting capacity and accumulated in JIMT-1 cell-bearing mice. However, accumulation did not occur in the organs of xenograft mice. Additionally, marmosets showed rapidly decrease in radioactivity throughout the entire body without accumulation in the normal organs. We also confirmed that the drug distribution was similar in normal organs between the two experimental animal species except spleen. Therefore, $^{125}$I is expected to be a useful tool in the study of RI-ADME in biopharmaceuticals through minimal antibody modification.**

**Key words:** radioisotope ADME (RI-ADME), biodistribution, trastuzumab-monomethyl auristatin F (trastuzumab-MMAF), single-photon emission computed tomography/computed tomography (SPECT/CT), marmoset

## Introduction

Radioisotope ADME (RI-ADME) studies are performed to evaluate the *in vivo* absorption, distribution, metabolism, and excretion of radiolabelled compounds in the body [1]. Since numerous novel therapeutic antibodies have appeared in new drug development pipelines, antibodies labelled with positron-emitting radioisotopes or gamma ray-emitting radioisotopes can be used for acquiring quantitative images for the *in vivo* behaviour of drugs through molecular imaging. These antibodies are also widely applied in pharmacokinetic (PK) studies to quantify the distribution of drugs in target and normal organs [2−4].

Molecular imaging methods such as radiotracer-based single-photon emission computed tomography/computed tomography (SPECT/CT) can visualize the *in vivo* behaviour of radiolabelled compounds in a non-invasive manner. Particularly, in preclinical studies, imaging studies in live animals have many advantages. Real-time dynamics of the biodistribution of radiolabelled compounds can be obtained in the same animal and the number of animals used in the study can be minimized. Thus, these tools are essential for ADME evaluation of new drug candidates [2, 5, 6]. Radioisotopes used to radiolabel antibodies are typically composed of radiometals and radio-

***Corresponding author:** Dong Hwan Kim
Department of Medicinal Biosciences, Konyang University, Nonsan 32992, Korea
Tel: +82-42-730-5425, E-mail: dhkim@konyang.ac.kr

halogens. Metallic radionuclides such as $^{90}$Y, $^{111}$In, $^{177}$Lu and $^{99m}$Tc can be used to label antibodies via coordination bonds with functional group of proteins or chelators [7, 8−10].

However, most monoclonal antibodies do not contain metal coordination sites, which reduces the stability of the antibody following metal radionuclide labelling. To overcome this obstacle, bifunctional chelators are attached to metal radionuclides. As metal radionuclides have varying coordination chemistries and properties for each radioisotope, a bifunctional chelator suitable for each isotope must be applied. Additionally, the coordination chemistry of metal radionuclides can affect the stability and geometry of radiometal chelators [8, 9, 11, 12].

Radiohalogens such as radioiodine, can directly label the tyrosine or histidine residues of monoclonal antibodies without chelator conjugation via stable covalent bonds. In addition, the steric and electronic properties of radiohalogens are expected to cause minimal modifications to proteins while showing very high specific activity [10, 11, 13, 14].

Radiohalogens are most often, particularly radioiodines, used to label antibodies since (1) the stable binding forms of radioiodine cause minimal changes and increase stability of the protein backbone, (2) the labelling methods are simple, (3) their chemistry is well characterized, (4) they allow for high radiochemical purity and specific activity, and (5) demonstrate a relatively long half-life. Hence, radioiodine labelling of biomolecules has been widely applied to studies, including those for screening new drug candidates in radio-immuno assays and preclinical ADME studies [7, 10, 13, 15−17].

The most commonly used radioiodines are $^{123}$I, $^{124}$I, $^{125}$I, and $^{131}$I [7]. Since $^{125}$I emits the lowest gamma ray energy (27−32 keV) and has the longest half-life ($t_{1/2}$ = 59.4 days) among commonly used radioiodines, it is expected to cause minimal radiation damage to labelled antibodies. $^{125}$I is also the first radioisotope to be considered for preclinical biodistribution studies of radiolabelled antibodies due to its high specific activity, relatively low cost, well-characterized iodination chemistry, and long half-life [2, 14, 18]. Particularly, $^{125}$I is used for antibody labelling to reveal metabolic pathways in sacrificed animals by gamma-counter and is mainly used for PK, SPECT imaging, and *in vivo* studies [7, 19, 20]. Therefore, we selected $^{125}$I to evaluate its *in vivo* behavior and to perform imaging studies for up to 3 weeks in this study.

Trastuzumab (herceptin; Genentech, South San Francisco, CA, USA) is the first HER2-targeting recombinant humanized monoclonal antibody approved by the Food and Drug Administration for treating patients with HER2-overexpressing metastatic breast cancer. It significantly increases the survival rate of patients and has been used to treat early stage and metastatic breast cancers [21−23]. However, many patients show intrinsic resistance to trastuzumab. Additionally, patients showing clinical effects early in treatment have experienced disease progression within one year of treatment because of the development of resistance to long-term treatment [24−26].

Recently, many targeted therapy studies have been conducted to treat cancer more effectively and safely. In this type of therapy, specific targeted molecules selectively act only on cancer cells to block their rapid division [27]. An antibody-drug-conjugate (ADC) is a structure that combines a monoclonal antibody with cytotoxic payload using a linker and has shown excellent therapeutic effects in clinical trials [28−30].

Currently, tubulin inhibitors (MMAE, MMAF, DM1, DM4) are widely used as ADCs with cytotoxic payload delivery to tumor tissues. Particularly, monomethyl auristatin (MMAE, MMAF) is the most commonly used and is applied in nearly 50% of clinical studies. Monomethyl auristatin F (MMAF) is used as cytotoxic payload in nine ADCs, including ADCs targeting the HER2 antigen, and is actively being evaluated in clinical studies [31−33]. MMAF is a very stable molecule that is not degraded in the plasma, human liver lysosomes, and by proteases such as cathepsin B [34] and shows excellent efficacy and high stability in ADCs [35]. The test substance LCB14-0110 used in this study is an ADC with indications for HER2-positive breast cancer. LCB14-0110 is comprised of MMAF conjugated to trastuzumab.

Two animal species were used for RI-ADME studies. Xenograft model mice without immune cells into which patient-derived tumors or cell lines are transferred are commonly used in preclinical studies to examine the anticancer effects of drugs [36, 37]. The common marmoset monkey (*Callithrix jacchus*) is a small non-human primate (NHP) that is more similar to humans than to rodents in its anatomical structure, genetic and physiological functions, and metabolism. Compared to larger NHPs, it has a large body surface area, which requires a rapid metabolic rate and small amount of test substance, thereby saving both time and money. Thus, marmosets are being increasingly used in preclinical studies [38−40]. In fact, marmoset monkeys have been evaluated in PK (ADME) studies, in toxicity evaluations of new drug candidates, cognitive studies, and pharmacodynamics analyses (neuroscience, immunology, infectious disease) [40, 41].

In this study, after labelling LCB14-0110 with $^{125}$I to minimize antibody structural alterations, gamma-counter and SPECT/CT imaging were performed to evaluate the

human breast cancer tumor targeting and biodistribution of $^{125}$I-LCB14-0110 in HER2-positive breast cancer cell-bearing mice. In addition, we evaluated the biodistribution and accumulation of $^{125}$I-LCB14-0110 in normal organs in healthy marmoset monkeys.

## Materials and Methods

### Antibody and reagents

LCB14-0110 was used as a trastuzumab-MMAF and provided by LegoChem Biosciences (Daejeon, Korea). As reagents for radioisotope labelling, chloramine-T and sodium metabisulfite were obtained from Sigma Aldrich (St. Louis, MO, USA). [$^{125}$I]NaI was purchased from Saehan Industry (Seoul, Korea). High-purity tertiary distilled water (deionized water, 18.2 MΩ, Millipore, Billerica, MA, USA) was used. A plate for radio-thin-layer chromatography (TLC; Silica gel 60 F254-25 aluminum sheets 20 × 20 cm) was purchased from Merck (Darmstadt, Germany).

### Radiolabelling

For the radiolabelling, modified Ma's method was used [42]. Briefly, LCB14-0110 was directly labelled with radioiodine by electrophilic aromatic substitution of tyrosine residues without chelator conjugation. Chloraimine-T (10 $\mu$L, 30 $\mu$g in phosphate-buffered saline; PBS) and 1 mCi of [$^{125}$I]NaI were added to 1 mL of LCB14-0110 (0.15 mg/mL). The reaction was performed at room temperature for 90 s. Next, 10 $\mu$L of sodium metabisulfite solution (90 $\mu$g in PBS) was added to quench the radioiodine reaction. The radiolabelled drug was purified using a PD-10 column. The developing solvent was acetone. The radiochemical purity was determined by radio-TLC analysis (AR-2000, BIOSCAN, Poway, CA, USA).

### Cell culture

The human breast cancer cell line JIMT-1 (HER2- positive) was purchased from Addexbio (San Diego, CA, USA). JIMT-1 cells were incubated in Dulbecco's Modified Eagle Medium containing 1% antibiotics + pyruvate (Gibco, Grand Island, NY, USA) and 10% fetal bovine serum. Subcultures were performed every 3–4 days at a 1:5 ratios. The cells were incubated in a humidified atmosphere containing 37℃ and 5% $CO_2$.

### *In vitro* stability

To evaluate the *in vitro* stability of $^{125}$I-LCB14-0110, experiments were performed in PBS, mouse serum, and human serum. First, 100 $\mu$L of $^{125}$I-LCB14-0110 (30 $\mu$Ci) was added to 400 $\mu$L of PBS, mouse serum, and human serum and then reacted at room temperature for 0, 1, 3, 7, 14, and 21 days. Stability analysis was performed over time by radio-TLC.

### Pharmacokinetic studies

All animal studies were approved by the Osong Medical Innovation Foundation Animal Care and Use Committee (KBIO-IACUC-2019-047 & 048) and were conducted in accordance with the guidelines of the committee.

#### 1) Tumor-bearing mice

Five-week-old female BALB/c-nude mice were purchased from Orient Bio (Gyeonggi, Korea). The mice were inoculated subcutaneously into the right flank with 0.2 mL solution containing 2 × $10^6$ JIMT-1 cells in PBS (100 $\mu$L) with 100 $\mu$L of Matrigel (Corning, Corning, NY, USA). When the mean tumor volume reached approximately 200 mm$^3$, the animals were used for *in vivo* studies.

#### (1) Blood PK

The blood PK of $^{125}$I-LCB14-0110 was evaluated in JIMT-1 tumor-bearing mice (n = 3/time point). Blood was collected at each time point (1 and 6 h, 1, 3, 7, 14, and 21 days) after intravenous administration 2 $\mu$Ci (154 ng/mice) of $^{125}$I-LCB14-0110 to xenograft mice.

Phoenix® WinNonlin® 8.0 version, Certara, St. Louis, MO, USA) was used for noncompartmental PK analysis. The half-life ($t_{1/2}$), clearance (CL), volume of distribution (Vd), area under the blood concentration-time curve from time zero to the last measurable concentration ($AUC_{last}$), and area under the blood concentration-time curve from time zero to infinity ($AUC_{inf}$) were calculated. PK parameters values are expressed as the mean ± S.D.

#### (2) Biodistribution

To assess the biodistribution of $^{125}$I-LCB14-0110 in JIMT-1 tumor-bearing mice, samples of major organs (heart, spleen, liver, stomach, kidney, intestine, lung, thyroid) and tumors were harvested following sacrifice under inhalation anesthesia (1%–2% of isoflurane in 1 L/min of oxygen) at each time point (1 and 6 h, 1, 3, 7, 14, and 21 days).

Radioactivity in each organ was measured with a gamma-counter (2480 WIZARD2, PerkinElmer, Waltham, MA, USA). Biodistribution results were expressed by calculating the percentage of the injected dose per gram of tissue (%ID/g, mean ± S.D.).

#### (3) SPECT/CT imaging

After intravenous administration of 400 $\mu$Ci $^{125}$I- LCB14-0110 (30 $\mu$g/head) in JIMT-1 tumor-bearing mice (n = 2), SPECT/CT images were obtained using small animal

SPECT/CT (Nano PET/CT, Mediso, Budapest, Hungary). Under inhalation anesthesia (1%–2% of isoflurane in 1 L/min of oxygen), CT images were acquired to obtain anatomical information. SPECT images were acquired at different time points (1 h, 1, 3, 7, 14, and 21 days), and whole-body images were obtained with 20% energy windows using a multi pinhole collimator.

### 2) Healthy marmoset monkey

#### (1) Biodistribution

The biodistribution of $^{125}$I-LCB14-0110 was evaluated in female healthy common marmoset (n = 2, body weight = n1: 304, n2: 298 g). Blood was collected from the femoral vein at one day after intravenous administration of 10 $\mu$Ci $^{125}$I-LCB14-0110 (0.77 μg/head). Subsequently, the marmosets were sacrificed under anesthesia, and major organs (heart, spleen, liver, stomach, kidney, intestine, lung) were collected. Biodistribution study was carried out as described above for tumor-bearing mice.

#### (2) SPECT/CT imaging

After intravenous administration of 700 $\mu$Ci $^{125}$I-LCB14-0110 (54 $\mu$g/head) to healthy common marmoset female monkey (n = 2, body weight = 369(n1), 327(n2) g), SPECT/CT images were obtained by small animal SPECT/CT (Nano PET/CT, Mediso). Cardiac anesthesia was induced by intravenous administration of 30 mg/kg zoletil and 10 mg/kg rompun before SPECT/CT imaging. Under inhalation anesthesia (2%–2.5% of isoflurane in 1 L/min of oxygen) CT images were acquired for anatomical analysis. SPECT images were taken at different time points (1 h, 1, 3, 7, 14, and 21 days), and whole-body images were obtained with 20% energy windows using a multi pinhole collimator.

### Statistical analysis

All experiments data are expressed as the mean ± S.D.

## Results

### Radiolabelling ($^{125}$I-LCB14-0110)

Radio-TLC was performed to confirm labelling of LCB14-0110, with acetone used as the developing solvent. Free $^{125}$I showed a retention factor (Rf) of 0.99 and radiolabelled $^{125}$I-LCB14-0110 had an Rf value of 0.01. The radiochemical purity was 100% (Fig. 1).

### *In vitro* stability

To evaluate the stability of $^{125}$I-LCB14-0110, 100 $\mu$L of $^{125}$I-LCB14-0110 (30 $\mu$Ci) was added to 400 $\mu$L of PBS, mouse serum, and human serum and allowed to react at room temperature for 3 weeks. The reactions were analysed over time by radio-TLC.

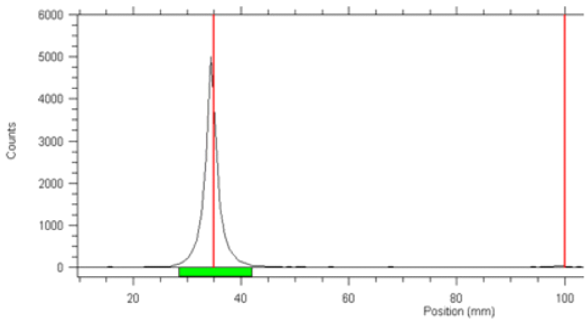


**Fig. 1.** Thin-layer chromatography of $^{125}$I-LCB14-0110.

$^{125}$I-LCB14-0110 showed high stability of approximately 100% in PBS, mouse serum, and human serum up to day 3. On day 7, stability in PBS was 98.71%, in mouse serum was 99.08%, and in human serum was 100%. On day 14, stability values were 97.24%, 98.11%, and 98.65%. on day 21, these values were 94.86%, 98.7%, and 98.03%, respectively.

Free $^{125}$I accounted for less than 5% of the total $^{125}$I-LCB14-0110 over three weeks (Fig. 2), and no significant difference over time was observed. $^{125}$I-LCB14-0110 showed high stability *in vitro*.

### PK studies

#### 1) Tumor-bearing mice

#### (1) Blood PK

The blood PK parameters of $^{125}$I-LCB14-0110 were calculated by collecting blood at different time points (1 and 6 h, 1, 3, 7, 14, and 21 days) after intravenous administration of $^{125}$I-LCB14-0110 in JIMT-1 human breast cancer xenograft mice (Fig. 3). The blood PK parameter was calculated from the average value of the sampling time point using three animals at each time point. The results showed the highest radioactivity at 1 h after

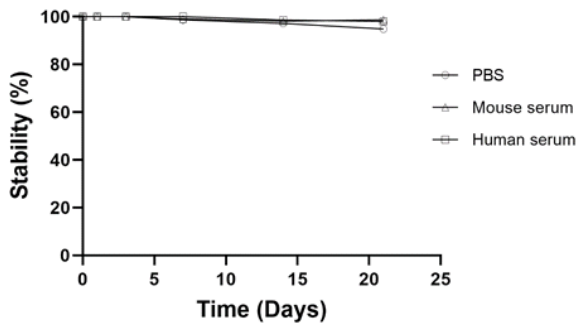


**Fig. 2.** *In vitro* stability of $^{125}$I-LCB14-0110 in PBS, mouse serum, and human serum.

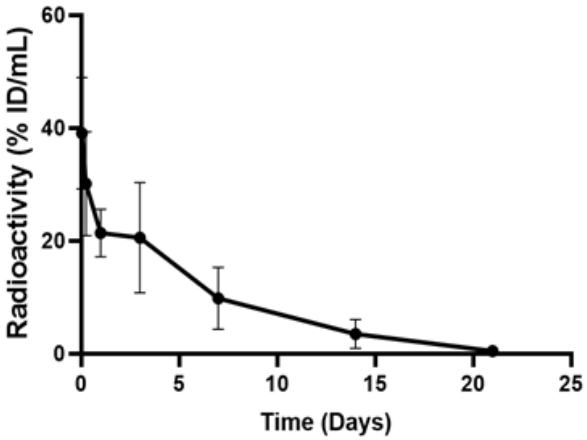


**Fig. 3.** Average blood radioactivity concentration vs time curve obtained after intravascular injection of 2 $\mu$Ci $^{125}$I-LCB14-0110 (154 ng/mice) in HER2-positive JIMT-1 cell-bearing mice. Values are represented as the mean % ID/mL ± S.D. (% ID/mL: percent injected dose per milliliter of blood).

administration (39.06 ± 8.08% ID/g). After this time, the radioactivity was distributed to organs over time, showing a 99% reduction at 0.46 ± 0.19% ID/g on day 21.

Blood PK parameters are shown as the half-life ($t_{1/2}$): 82.71 h, area under the concentration-time curve from time zero to the last measurable concentration ($AUC_{last}$): 4,331.65 (% ID × h/mL), area under the concentration-time curve from time zero to infinity ($AUC_{inf}$): 4,374.46 (% ID × h/mL), volume of distribution: 4.20 (mL/kg), and CL: 0.035 (mL/h/kg).

### (2) Biodistribution

The biodistribution was evaluated for 21 days after intravenous administration of 2 $\mu$Ci $^{125}$I-LCB14-0110 (154 ng/mouse) in HER2-positive JIMT-1 cell-bearing mice with a gamma-counter. As a result, the tumor showed the highest uptake at day 3 which increased by approximately 300% compared to at 1 h (1 h: 3.23 ± 1.41% ID/g, day 3: 12.96 ± 5.36% ID/g). We observed increased uptake into the tumor for up to 3 days, followed by a decrease from 7$^{th}$ day (Fig. 4). The kidneys and lungs in normal organs showed relatively high radioactivity at 1 h (9.37 ± 3.43% ID/g, 14.25 ± 3.55% ID/g, respectively), but showed lower radioactivity than the tumors at day 1 (kidney: 4.61 ± 0.88 %ID/g, lung: 8.09 ± 0.74 %ID/g, tumor: 9.22 ± 0.75% ID/g) and so on. At 6 h, radioactivity was increased in the spleen, stomach, and intestine compared to at 1 h, but thereafter showed a sharp decrease over time.

Comparing the radioactivity of tumor and blood (Fig. 5), LCB14-0110 was targeting to the tumor and the tumor to blood ratio (T/B ratio) was gradually increased over time.

### (3) Small animal SPECT/CT imaging

Small animal SPECT/CT images were acquired at 1 h, 1, 3, 7, 14, and 21 days after intravenous administration of 400 $\mu$Ci $^{125}$I-LCB14-0110 (30 $\mu$g/mouse) in HER2-positive JIMT-1 cell-bearing mice (Fig. 6).

Uptake was high in the heart, liver, lung, and kidney at 1 h, and then decreased over time. On 14$^{th}$ day, $^{125}$I-LCB14-0110 had lost much radioactivity in the whole body. On 21$^{th}$ day, nearly no radioactivity remained in the body except for in the thyroid and tumor. The tumor

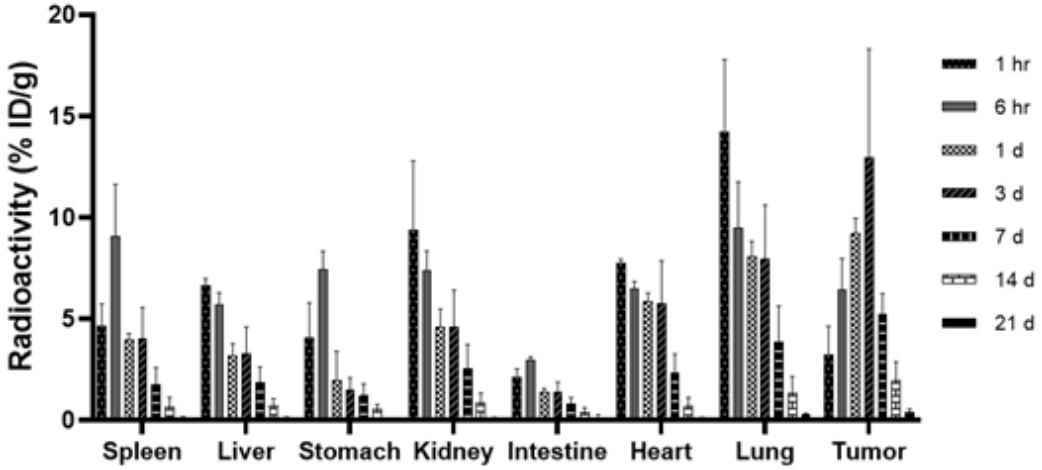


**Fig. 4.** Biodistribution results of intravenous administrated 2 $\mu$Ci $^{125}$I-LCB14-0110 (154 ng/mouse) in HER2-positive JIMT-1 cell-bearing mice. Radioactivity in normal organs and tumor was measured at 1 and 6 h, 1, 3, 7, 14, and 21 days after injection $^{125}$I-LCB14-0110. Radioactivity in tissues is expressed as %ID/g. Radioactivity in thyroid is excluded in this graph.

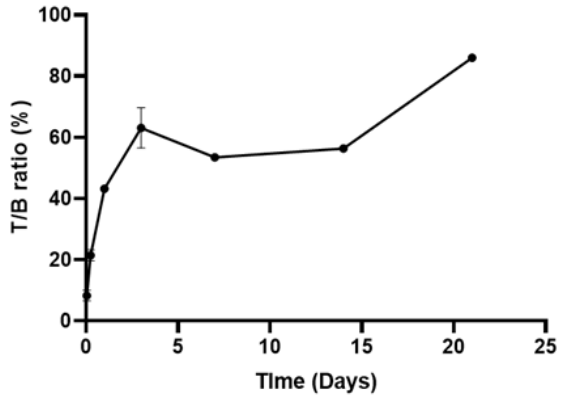


**Fig. 5.** The tumor to blood ratio (T/B ratio) of radioactivity from HER2-positive JIMT-1 cell-bearing mice after intravenous administration of 2 $\mu$Ci $^{125}$I-LCB14-0110 (154 ng/mouse). The radioactivity was measured at 1 and 6 h, 1, 3, 7, 14, and 21 days after dosing.

showed increased uptake over time starting on day 1, with the highest uptake and accumulation found on day 3.

### 2) Healthy marmoset monkey

#### (1) Biodistribution

To evaluate the biodistribution of $^{125}$I-LCB14-0110 in normal animals, 10 $\mu$Ci (0.77 μg/head) of $^{125}$I-LCB14-0110 was intravenously administered to healthy marmosets. After blood was collected on day 1, sacrificed marmosets were assessed for biodistribution study using a gamma-counter (Fig. 7). As a result, the highest uptake was found in the spleen (n1: 2.31, n2: 4.22% ID/g), and other organs showed low radioactivity of less than approximately 1% ID/g.

#### (2) Small animal SPECT/CT imaging

Whole-body small animal SPECT/CT images were ac-

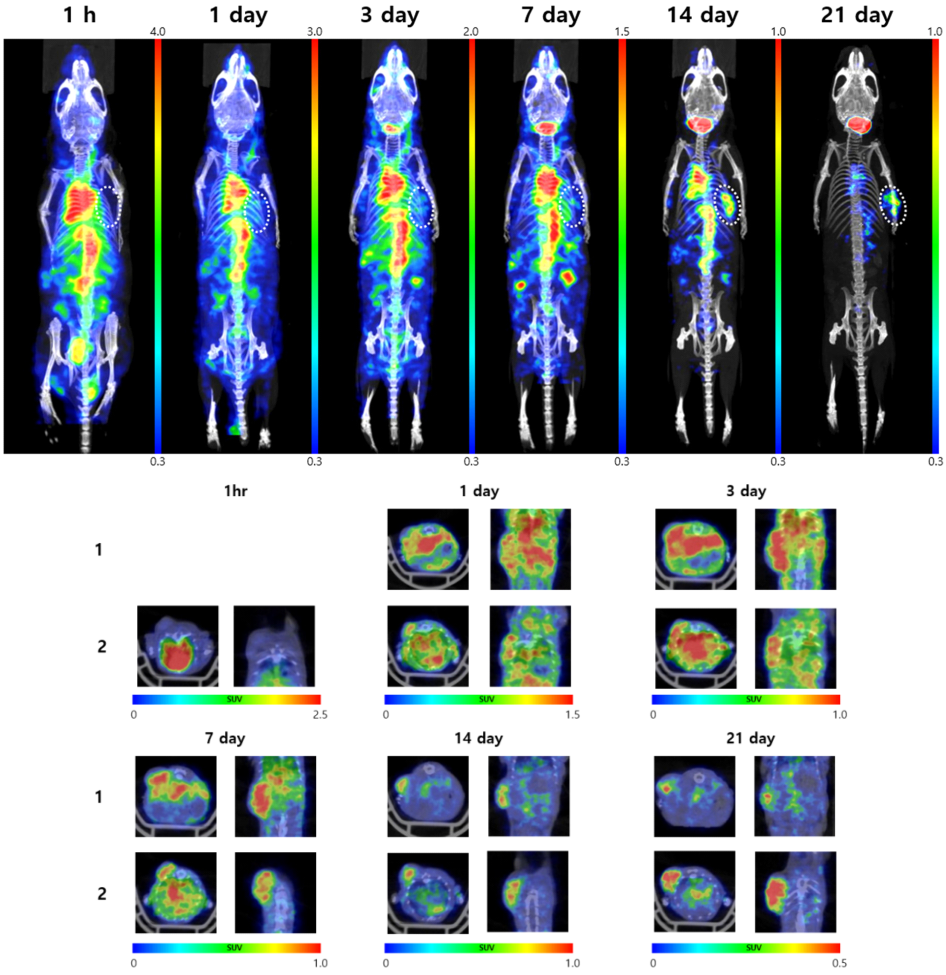


**Fig. 6.** Whole-body small animal SPECT/CT images at 1 h, 1, 3, 7, 14, and 21 days after intravenous administration of 400 $\mu$Ci $^{125}$I-LCB14-0110 (30 $\mu$g/mouse) in HER2-positive JIMT-1 cell-bearing mice. Images show biodistribution, clearance and tumor targeting of $^{125}$I-LCB14-0110. Upper images are the coronal plane of the mouse. White dotted lines indicated tumor site. Lower images are the transverse plane of the mouse. SPECT/CT, single-photon emission computed tomography/computed tomography.

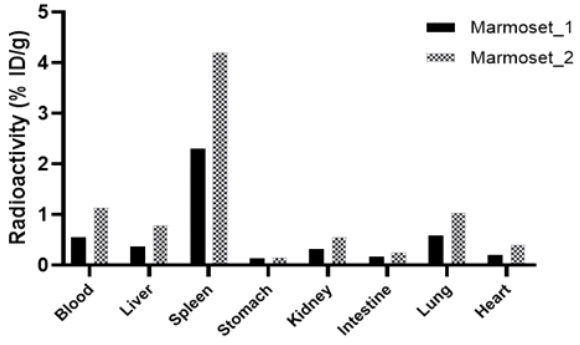


**Fig. 7.** Biodistribution results of intravenous administrated 10 μCi $^{125}$I-LCB14-0110 (0.77 μg/head) in two healthy marmosets. Radioactivity in normal organs was measured on day 1 after injection $^{125}$I-LCB14-0110. Radioactivity in the tissues is expressed as % ID/g.

quired at 1 h, 1, 3, 7, 14, and 21 days after intravenous administration of 700 $\mu$Ci $^{125}$I-LCB14-0110 (54 $\mu$g/head) in healthy marmosets. Relatively high uptake was observed in the heart, liver, stomach, kidney, and spleen at 1 h (Fig. 8). Except for the thyroid gland, whole-body radioactivity rapidly decreased starting at 3 days, and most radioactivity administered was excreted within 1 week. The results confirmed no radioactivity accumulation in the normal organs.

### Comparison of radioactivity distribution in the organs of tumor-bearing mice and healthy marmoset

Based on the biodistribution results described in section 3.3.1.2 tumor-bearing mice and section 3.3.2.1 in healthy marmoset, the distribution of radioactivity in the normal organs in the two animal species at day 1 after $^{125}$I-LCB14-0110 administration was compared. We calculated the % ID/tissue considering the difference in organ weight of the mice and marmoset (Table 1). The xenograft mice showed higher distribution in the blood and intestine than marmosets. Whereas, the radioactivity of spleen and liver of marmoset was higher than those of tumor-bearing nude mice. Other organs showed similar distributions in the two animal species.

## Discussion

After labelling radioiodine with antibodies to minimize modification of the antibody structure in LCB14-0110, we evaluated the tumor targets and *in vivo* behavior by gamma-counter and SPECT/CT imaging. In this study, $^{125}$I-LCB14-0110 showed a high radiochemical purity and high stability for 3 weeks in both mouse and human serum. Based on these results, radioiodine labelling of the ADC in this study was useful for *in vivo* imaging and long-term PK studies. Therefore, *in vivo* studies were conducted. To evaluate the tumor targeting ability and *in vivo* behavior of $^{125}$I-LCB14-0110 (HER2 Targeting anticancer agent), PK analysis and biodistribution studies in tumor-bearing mice and healthy marmoset monkeys were performed by gamma-counter, with *in vivo* behavior images obtained by using SPECT/CT. Xenograft mice and marmosets were administered intravenously with specific activity (13 $\mu$Ci/1 $\mu$g) for using optimized dose in

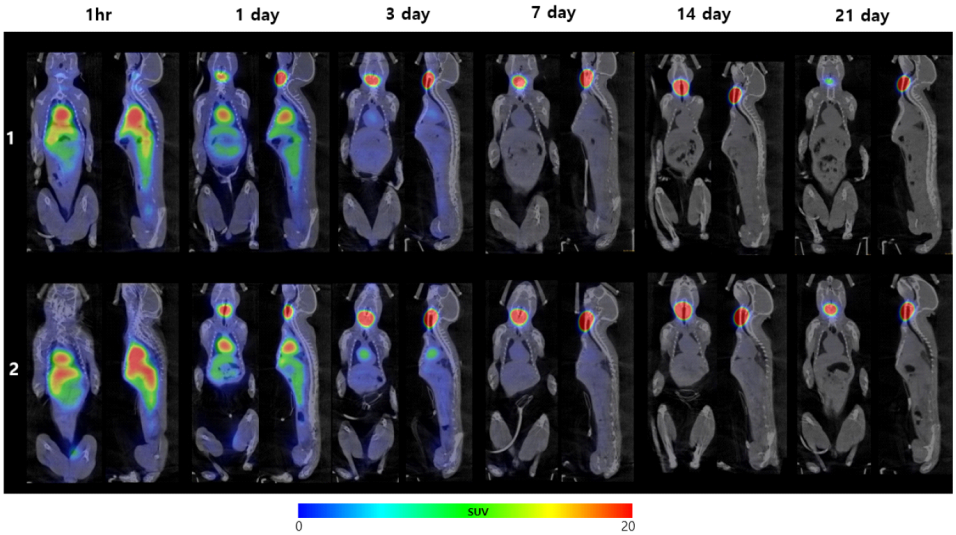


**Fig. 8.** Whole-body small animal SPECT/CT images at 1 h, 1, 3, 7, 14, and 21 days after intravenous administration of 700 $\mu$Ci $^{125}$I-LCB14-0110 (54 $\mu$g/head) in healthy marmosets. The image shows the biodistribution and clearance of $^{125}$I-LCB14-0110. SPECT/CT, single-photon emission computed tomography/computed tomography.

**Table 1.** Comparison of organ biodistribution in HER2-positive JIMT-1 cell-bearing mice and healthy marmosets at day 1 after administration of $^{125}$I-LCB14-0110. Radioactivity is expressed as % ID/tissue

| Organs | Tumor bearing mice | | Healthy marmoset | |
|---|---|---|---|---|
| | % ID/tissue | Relative organ weight (%) | % ID/tissue | Relative organ weight (%) |
| Blood | 31.770 ± 10.869 | 7* | 17.743 ± 8.648 | 7* |
| Liver | 3.809 ± 1.211 | 5.68 ± 0.40 | 5.939 ± 2.838 | 3.15 ± 0.17 |
| Spleen | 0.466 ± 0.020 | 0.58 ± 0.10 | 0.729 ± 0.090 | 0.07 ± 0.01 |
| Heart | 0.568 ± 0.108 | 0.48 ± 0.05 | 0.523 ± 0.273 | 0.51 ± 0.01 |
| Kidneys | 1.195 ± 0.408 | 1.21 ± 0.08 | 0.784 ± 0.295 | 0.55 ± 0.08 |
| Lung | 1.111 ± 0.297 | 0.63 ± 0.04 | 1.154 ± 0.548 | 0.43 ± 0.08 |
| Stomach | 0.765 ± 0.538 | 2.18 ± 0.70 | 0.170 ± 0.006 | 0.36 ± 0.01 |
| Intestine | 3.513 ± 0.905 | 11.89 ± 0.87 | 2.650 ± 0.322 | 2.60 ± 0.79 |

* Blood volume was estimated 7% of total body weight for calculation.

biodistribution study and SPECT/CT imaging. Stollman *et al*. reported that addition of unlabelled antibodies to labelled antibodies significantly reduced the amount of labelled antibody targeted to tumors when adjusted to the clinical dose [43]. Accordingly, we used the optimal radioactivity dose rather than the clinical dose of $^{125}$I-LCB14-0110 to confirm tumor targeting.

Biodistribution evaluation using a gamma-counter in tumor bearing mice showed the highest uptake and accumulation at day 3, with radioactivity increasing over time in the tumor. Additionally, increasing the T/B ratio may have greatly affected the tumor-targeting ability.

In normal organs of tumor-bearing mice, uptake by the lung and kidney was relatively high at 1 h. At 6 h, increased radioactivity was observed in the spleen, stomach, and intestine compared to at 1 h. Healthy marmosets showed the highest uptake in the spleen (n1: 2.31, n2: 4.22% ID/g) at day 1. Increasing radioactivity in the stomach and intestine of tumor bearing mice has previously been reported for gastric radioiodine accumulation which occurs because of the *in vivo* catabolism and deiodination of labelled antibodies when using iodine direct labelling [7, 44]. Accordingly, we determined that transiently high uptake in the stomach and intestines occurred because of radiolabelling.

In addition, the lung, spleen, and kidney of tumor-bearing mice showed high radioactivity. This results were similar to those of other studies in which trastuzumab was administered to HER2-positive tumor-bearing mice [45−47]. According to Yang *et al*. [46], trastuzumab showed high uptake in the spleen and kidneys, which are organs of the reticuloendothelial system (RES) and detects external substances based on sufficient blood flow and metabolism. Additionally, the lungs are generally known to exhibit acute accumulation after trastuzumab administration and showed temporary high uptake of radioactivity in this study [48]. Other normal organs and blood showed continuous decreases in radioactivity over time.

Small animal SPECT/CT imaging revealed high uptake in the heart, liver, lung, and kidney at 1 h post-administration of $^{125}$I-LCB14-0110 in tumor-bearing mice. These results are consistent with the high uptake by normal organs at the same time point in the biodistribution study. SPECT/CT imaging showed a rapid decrease in radioactivity at day 14, with very low radioactivity in the whole body except for in the tumor and thyroid areas on day 21. Whereas radioactivity in the whole body and major organs decreased over time, in tumors, radioactivity increased gradually until day 3, showing the highest uptake at this time point. Intratumoral radioactivity was observed until 21 days, confirming tumor targeting and accumulation. The biodistribution results were similar to the tumor SPECT/CT imaging results and to those of another study of the correlation between SPECT/CT imaging and biodistribution [49], confirming the relation between the biodistribution and SPECT/CT imaging of $^{125}$I-LCB14-0110 in tumor-bearing mice. Our results confirmed the tumor targeting profile and distribution profile in normal organs.

Marmosets showed higher uptake of radioactivity in the spleen than in the other normal organs. Similar results were obtained from other studies comparing the biodistribution of $^{64}$Cu-labelled trastuzumab in mice with HER2-positive breast tumors and normal mice. The results showed that in normal mice, the spleen had the highest uptake of radioactivity among normal organs

[50]. Clinical studies showed similar results. Whole body PET imaging results at 1, 24, and 48 h after injection $^{64}$Cu-1,4,7,10-tetraazacyclododecane-1,4,7,10-tetraacetic acid-trastuzumab in HER2-positive breast cancer patients revealed significantly higher accumulation in the spleen at all-time points. These results indicate that monoclonal antibodies interact with specific antigens or are specifically captured by splenic macrophages, causing accumulation in the spleen [51, 52].

SPECT/CT imaging results in marmosets showed relatively high radioactivity in the heart, spleen, liver, stomach, and kidney on day 1. The difference from the biodistribution results was less than 3% ID/g. The similarity of uptake in normal organs was confirmed in the biodistribution study and SPECT/CT imaging results. Particularly, SPECT/CT imaging showed high uptake in the heart at 1 h. Radioactivity in the heart, where large blood vessels are located, was higher than that observed by gamma counting, which revealed radioactivity after tissue extraction and perfusion [53]. After 3 days of administration, whole-body radioactivity except for in the thyroid was rapidly reduced, with no accumulation in normal organs.

Comparison of the distribution of radioactivity in normal organs between two animal species at the same time point (1 day post-administration) showed that LCB14-0110 had a far lower spleen uptake (more than 13 times lower considering organ weights) and relatively higher (1.8 fold) blood radioactivity in nude mice than healthy marmosets. These differences may be caused by the role of filtering the antigen in the spleen was reduced due to lack of immunity. Accordingly, the overall loss of radioactivity is also observed more rapidly in the marmoset.

In addition, T-DM1 was found to be toxic in the spleen of Sprague-Dawley rats and cynomolgus monkeys and was accompanied by RES hypertrophy as well as lymphocyte necrosis and degeneration [54], with similar results found in clinical studies. Magnetic resonance imaging of patients with metastatic breast cancer treated with T-DM1 indicated an increase in the average spleen size from 144 $cm^3$ (95% CI 110−177 $cm^3$) to 209 $cm^3$ (95% CI 161−257 $cm^3$) in 92% of patients [55]. This indicates that the conjugated drug of ADC is degraded in the antibody and then released and accumulates in the spleen [56]. The high radioactivity in the spleen of marmosets in this study was thought to occur for this reason. Whereas, relatively low distributions were observed in other normal organs of marmosets.

Comparison of the results of clinical studies of trastuzumab and biodistribution of LCB14-0110 marmosets revealed similarities, with higher uptake in the spleen. As described by Smith et al and Hart *et al*. [39, 57], marmosets have similar metabolism and immune systems as humans, and thus show similar biodistributions of drugs. Therefore, marmosets are useful for predicting the human biodistribution of test substances in ADME research in the new drug development process.

We confirmed the effective tumor targeting and accumulation of $^{125}$I-LCB14-0110 in HER2-positive tumor-bearing mice and verified continued reduction of radioactivity in the blood and normal organs over time. Radioactivity rapidly decreased in healthy marmosets without targeting normal organs. Additionally, the distribution of each organ of $^{125}$I-LCB14-0110 in mice and marmoset was similar except spleen. In conclusion, $^{125}$I used is expected to be a useful tool in the study of RI- ADME in biopharmaceuticals through minimal antibody modification.

## Acknowledgments

This study was supported by a grant (HO15C0001) from Osong Innovation Foundation funded by the Ministry of Health and Welfare, Korea.

## ORCID

Hye Won Lee, https://orcid.org/0000-0003-4806-4858
Yun Ha Jeong, https://orcid.org/0000-0001-7293-3326
Jin Ah Hwang, https://orcid.org/0000-0001-8329-3029
Jae Jun Lee, https://orcid.org/0000-0001-6174-786X
A-Ram Yu, https://orcid.org/0000-0001-7411-6522
Jung Ae Kang, https://orcid.org/0000-0001-6444-3618
Muhammad Asim Raza, https://orcid.org/0000-0003-4316-6628
Sang Hyun Park, https://orcid.org/0000-0001-8219-5283
Yun-Hee Park, https://orcid.org/0000-0002-7875-1299
Dong Hwan Kim, https://orcid.org/0000-0002-3887-7743

## References

1. Dalvie D. Recent advances in the applications of radioisotopes in drug metabolism, toxicology and pharmacokinetics. Curr Pharm Des 2000;6:1009-1028.
2. Xu X, Vugmeyster Y. Challenges and opportunities in absorption, distribution, metabolism, and excretion studies of therapeutic biologics. AAPS J 2012;14:781-91.
3. Waaijer SJH, Kok IC, Eisses B, Schröder CP, Jalving M, Brouwers AH, Lub-de Hooge MN, de Vries EGE. Molecular imaging in cancer drug development. J Nucl Med 2018;59:726-732.
4. Morais M, Ma MT. Site-specific chelator-antibody conjugation for PET and SPECT imaging with radiometals.

Drug Discov Today Technol 2018;30:91-104.

5. Hillman EMC, Amoozegar CB, Wang T, McCaslin AFH, Bouchard MB, Mansfield J, Levenson RM. *In vivo* optical imaging and dynamic contrast methods for biomedical research. Philos Trans A Math Phys Eng Sci 2011;369: 4620-4643.
6. Fischman AJ, Alpert NM, Rubin RH. Pharmacokinetic imaging: a noninvasive method for determining drug distribution and action. Clin Pharmacokinet 2002;41:581-602.
7. Sugiura G, Kühn H, Sauter M, Haberkorn U, Mier W. Radiolabeling strategies for tumor-targeting proteinaceous drugs. Molecules 2014;19:2135-2165.
8. Tornesello AL, Buonaguro L, Tornesello ML, Buonaguro FM. New insights in the design of bioactive peptides and chelating agents for imaging and therapy in oncology. molecules 2017;22:1282.
9. Brechbiel MW. Bifunctional chelates for metal nuclides. Q J Nucl Med Mol Imaging 2008;52:166-173.
10. Anderson WT, Strand M. Radiolabeled antibody: iodine versus radiometal chelates. NCI Monogr 1987;3:149-151.
11. Zhou H, Theil FP. ADME and translational pharmacokinetics/pharmacodynamics of therapeutic proteins. 1st ed. Hoboken: John Wiley & Sons; 2015.
12. Packard AB, Kronauge JF, Brechbiel MW. Metalloradiopharmaceuticals. In: Clarke MJ, Sadler PJ (eds.). A metalloradiopharmaceuticals II: diagnosis and therapy. 1st ed. New York: Springer; 1999. p. 45-115.
13. Gupta S, Batra S, Jain M. Antibody labeling with radioiodine and radiometals. Methods Mol Biol 2014;1141:147-157.
14. Wilbur DS. Radiohalogenation of proteins: an overview of radionuclides, labeling methods, and reagents for conjugate labeling. Bioconjug Chem 1992;3:433-470.
15. Hiltunen JV. Search for new and improved radiolabeling methods for monoclonal antibodies: a review of different methods. Acta Oncol 1993;32:831-839.
16. Adam MJ, Wilbur DS. Radiohalogens for imaging and therapy. Chem Soc Rev 2005;34:153-163.
17. Baillie TA. Metabolism and toxicity of drugs. Two decades of progress in industrial drug metabolism. Chem Res Toxicol 2008;21:129-137.
18. Vugmeyster Y, DeFranco D, Szklut P, Wang Q, Xu X. Biodistribution of [125I]-labeled therapeutic proteins: application in protein drug development beyond oncology. J Pharm Sci 2010;99:1028-1045.
19. Zhu J, Zhang B, Tian J, Wang J, Chong Y, Wang X, Deng Y, Tang M, Li Y, Ge C, Pan Y, Gu H. Synthesis of heterodimer radionuclide nanoparticles for magnetic resonance and single-photon emission computed tomography dual-modality imaging. Nanoscale 2015;7:3392-3395.
20. Makrigiorgos G, Adelstein SJ, Kassis AI. Auger electron emitters: insights gained from *in vitro* experiments. Radiat Environ Biophys 1990;29:75-91.
21. Asif HM, Sultana S, Ahmed S, Akhtar N, Tariq M. HER-2 Positive breast cancer: a mini-review. Asian Pac J Cancer Prev 2016;17:1609-1615.
22. Slamon DJ, Leyland-Jones B, Shak S, Fuchs H, Paton V, Bajamonde A, Fleming T, Eiermann W, Wolter J, Pegram M, Baselga J, Norton L. Use of chemotherapy plus a monoclonal antibody against HER2 for metastatic breast cancer that overexpresses HER2. N Engl J Med 2001; 344:783-792.
23. Dahabreh IJ, Linardou H, Siannis F, Fountzilas G, Murray S. Trastuzumab in the adjuvant treatment of early-stage breast cancer: a systematic review and meta-analysis of randomized controlled trials. Oncologist 2008;13:620-630.
24. Ellis LM, Hicklin DJ. Resistance to targeted therapies: refining anticancer therapy in the Era of molecular oncology. Clin Cancer Res 2009;15:7471-7478.
25. Massicano AVF, Marquez-Nostra BV, Lapi SE. Targeting HER2 in nuclear medicine for imaging and therapy. Mol Imaging 2018;17:1536012117745386.
26. Nahta R, Yu D, Hung MC, Hortobagyi GN, Esteva FJ. Mechanisms of disease: understanding resistance to HER2-targeted therapy in human breast cancer. Nat Clin Pract Oncol 2006;3:269-280.
27. Chari RVJ. Targeted cancer therapy: conferring specificity to cytotoxic drugs. Acc Chem Res 2008;41:98-107.
28. Perez HL, Cardarelli PM, Deshpande S, Gangwar S, Schroeder GM, Vite GD, Borzilleri RM. Antibody-drug conjugates: current status and future directions. Drug Discov Today 2014;19:869-881.
29. Diamantis N, Banerji U. Antibody-drug conjugates: an emerging class of cancer treatment. Br J Cancer 2016; 114:362-367.
30. Dan N, Setua S, Kashyap VK, Khan S, Jaggi M, Yallapu MM, Chauhan SC. Antibody-drug conjugates for cancer therapy: chemistry to clinical implications. Pharmaceuticals (Basel) 2018;11:32.
31. Drake PM, Rabuka D. Recent developments in ADC technology: preclinical studies signal future clinical trends. BioDrugs 2017;31:521-531.
32. Johansson MP, Maaheimo H, Ekholm FS. New insight on the structural features of the cytotoxic auristatins MMAE and MMAF revealed by combined NMR spectroscopy and quantum chemical modelling. Sci Rep 2017;7:15920.
33. Nejadmoghaddam MR, Minai-Tehrani A, Ghahremanzadeh

R, Mahmoudi M, Dinarvand R, Zarnani AH. Antibody-drug conjugates: possibilities and challenges. Avicenna J Med Biotechnol 2019;11:3-23.

34. Tan C. Payloads of antibody-drug conjugates. In: Wang J, Shen W, Zaro JL (eds.). Antibody-drug conjugates: the 21st century magic bullets for cancer. 1st ed. New York: Springer; 2015. p. 11-22.

35. Humphreys RC, Kirtely J, Hewit A, Biroc S, Knudsen N, Skidmore L, Wahl A. Site specific conjugation of ARX-788, an antibody drug conjugate (ADC) targeting HER2, generates a potent and stable targeted therapeutic for multiple cancers. Cancer Res 2015;75:639.

36. Budhu S, Wolchok J, Merghoub T. The importance of animal models in tumor immunity and immunotherapy. Curr Opin Genet Dev 2014;24:46-51.

37. Cekanova M, Rathore K. Animal models and therapeutic molecular targets of cancer: utility and limitations. Drug Des Devel Ther 2014;8:1911-1921.

38. Phillips KA, Bales KL, Capitanio JP, Conley A, Czoty PW, 't Hart BA, Hopkins WD, Hu SL, Miller LA, Nader MA, Nathanielsz PW, Rogers J, Shively CA, Voytko ML. Why primate models matter. Am J Primatol 2014;76:801-827.

39. Smith D, Trennery P, Farningham D, Klapwijk J. The selection of marmoset monkeys *Callithrix jacchus* in pharmaceutical toxicology. Lab Anim 2001;35:117-130.

40. Orsi A, Rees D, Andreini I, Venturella S, Cinelli S, Oberto G. Overview of the marmoset as a model in nonclinical development of pharmaceutical products. Regul Toxicol Pharmacol 2011;59:19-27.

41. Zühlke U, Weinbauer G. The common marmoset *Callithrix jacchus* as a model in toxicology. Toxicol Pathol 2003;31: 123-127.

42. Ma S, Nam YR, Jeon J, Rho JK, Lee D, Choi DS, Jang B, Park SH. Simple and efficient radiolabeling of hyaluronic acid and its *in vivo* evaluation via oral administration. J Radioanal Nucl Chem 2015;305:139-145.

43. Stollman TH, Scheer MGW, Leenders WPJ, Verrijp KCN, Soede AC, Oyen WJG, Ruers TJM, Boerman OC. Specific imaging of VEGF-A expression with radiolabeled anti-VEGF monoclonal antibody. Int J Cancer 2008;122:2310-2314.

44. Goldenberg DM. Cancer therapy with radiolabelled antibodies. 1st ed. Boca Raton: CRC Press; 1995.

45. Terrell-Hall TB, Nounou MI, El-Amrawy F, Griffith JIG, Lockman PR. Trastuzumab distribution in an *in-vivo* and *in-vitro* model of brain metastases of breast cancer. Oncotarget 2017;8:83734-83744.

46. Yang ZX, Cao H, Xing CG, Wei SH, Jiang GQ, Liu ZL. Visualization and body distribution of [$^{131}$I]-herceptin in nude mice with BT-474 breast carcinoma. Genet Mol Res 2014;13:6804-6812.

47. Kobayashi H, Shirakawa K, Kawamoto S, Saga T, Sato N, Hiraga A, Watanabe I, Heike Y, Togashi K, Konishi J, Brechbiel MW, Wakasugi H. Rapid accumulation and internalization of radiolabeled herceptin in an inflammatory breast cancer xenograft with vasculogenic mimicry predicted by the contrast-enhanced dynamic MRI with the macromolecular contrast agent G6-(1B4M-Gd)$_{256}$. Cancer Res 2002;62:860-866.

48. European Medicines Agency. [EMA]. Annex I. Summary of product characteristics [annex to Herceptin: EPAR – Product Information] [Internet]. [cited 2019 Oct 14]. Available from: https://www.ema.europa.eu/documents/product-information/herceptin-epar-product-information_en.pdf

49. Finucane CM, Murray I, Sosabowski JK, Foster JM, Mather SJ. Quantitative accuracy of low-count SPECT imaging in phantom and *in vivo* mouse studies. Int J Mol Imaging 2011;2011:197381.

50. Woo SK, Jang SJ, Seo MJ, Park JH, Kim BS, Kim EJ, Lee YJ, Lee TS, An GI, Song IH, Seo Y, Kim KI, Kang JH. Development of 64Cu-NOTA-trastuzumab for HER2 targeting: a radiopharmaceutical with improved pharmacokinetics for human studies. J Nucl Med 2019;60:26-33.

51. Cataldi M, Vigliotti C, Mosca T, Cammarota M, Capone D. Emerging role of the spleen in the pharmacokinetics of monoclonal antibodies, nanoparticles and exosomes. Int J Mol Sci 2017;18:1249.

52. Tamura K, Kurihara H, Yonemori K, Tsuda H, Suzuki J, Kono Y, Honda N, Kodaira M, Yamamoto H, Yunokawa M, Shimizu C, Hasegawa K, Kanayama Y, Nozaki S, Kinoshita T, Wada Y, Tazawa S, Takahashi K, Watanabe Y, Fujiwara Y. 64Cu-DOTA-trastuzumab PET imaging in patients with HER2-positive breast cancer. J Nucl Med 2013;54:1869-1875.

53. Tian M, Lu W, Zhang R, Xiong C, Ensor J, Nazario J, Jackson J, Shaw C, Dixon KA, Miller J, Wright K, Li C, Gupta S. Tumor uptake of hollow gold nanospheres after intravenous and intra-arterial injection: PET/CT study in a rabbit VX2 liver cancer model. Mol Imaging Biol 2013; 15:614-624.

54. Poon KA, Flagella K, Beyer J, Tibbitts J, Kaur S, Saad O, Yi JH, Girish S, Dybdal N, Reynolds T. Preclinical safety profile of trastuzumab emtansine (T-DM1): mechanism of action of its cytotoxic component retained with improved tolerability. Toxicol Appl Pharmacol 2013;273:298-313.

55. Kosmin M, Makris A, Jawad N, Woolf D, Miles D, Padhani AR. Splenic enlargement and bone marrow hyperplasia in patients receiving trastuzumab-emtansine for metastatic breast cancer. Target Oncol 2017;12:229-234.

56. Han TH, Zhao B. Absorption, distribution, metabolism, and

excretion considerations for the development of antibody-drug conjugates. Drug Metab Dispos 2014;42:1914-20.

57. 't Hart BA, Abbott DH, Nakamura K, Fuchs E. The marmoset monkey: a multi-purpose preclinical and translational model of human biology and disease. Drug Discov Today 2012;17:1160-1165.